J Therm Spray Tech (2020) 29:1289–1299
https://doi.org/10.1007/s11666-020-01020-x

PEER REVIEWED

Correlation of Residual Stresses and Coating Properties in Arc-Sprayed Coatings on Different Substrates for Maritime Applications

Michél Hauer[1] · Sebastian Krebs[2] · Werner Kroemmer[3] · Knuth-Michael Henkel[4]

Submitted: 14 November 2019 / in revised form: 2 February 2020 / Published online: 31 March 2020

Abstract Arc spraying is a cost-effective technology, which is determined by a few key factors. It is already established for corrosion protection of large structures and thus considered for restoration of eroded ship rudders and propellers by depositing typical propeller materials. The main parameters like arc current, gas type/flow or process kinematics strongly influence the residual stresses in these coatings, which in turn affect coating properties. In past investigations, it was shown that this impact could be modified by using alternative gas mixtures or changing the heat input in the process. However, the mentioned studies neglect the influence of the substrate, since solely steel substrates were used. In consequence, propeller alloys CuAl9Ni5Fe4Mn (Ni-Al bronze) and CuMn13Al8Fe3Ni2 (Mn-Al bronze) were now arc-sprayed onto bronze substrates while using the same parameters and kinematics as in the past. For reproducible results, the residual stresses within the coatings were measured by novel incremental hole drilling method based on electronic speckle pattern interferometry (ESPI) and correlated with the other coating properties. In comparison with spraying onto steel, the same conditions led to reduced Young's moduli, lower tensile stresses and improved cavitation erosion resistance, while other properties like hardness and electrical conductivity showed varying trends.

Keywords aluminum bronze · cavitation-resistant coatings · electronic speckle pattern interferometry · marine components · residual stress determination · substrate coating interaction · wire arc spray

This article is part of a special topical focus in the *Journal of Thermal Spray Technology* on Advanced Residual Stress Analysis in Thermal Spray and Cold Spray Processes. This issue was organized by Dr. Vladimir Luzin, Australian Centre for Neutron Scattering; Dr. Seiji Kuroda, National Institute of Materials Science; Dr. Shuo Yin, Trinity College Dublin; and Dr. Andrew Ang, Swinburne University of Technology.

✉ Michél Hauer
michel.hauer@igp.fraunhofer.de;
michel.hauer@hro.ipa.fraunhofer.de

[1] Fraunhofer Institute for Large Structures in Production Engineering IGP - Welding Engineering, Rostock, Germany

[2] Helmut-Schmidt University, University of the Federal Armed Forces Hamburg - Material Science, Hamburg, Germany

[3] Linde AG – Linde Gases Division, Unterschleissheim, Germany

[4] Chair of Joining Technology, University of Rostock, Rostock, Germany

Introduction

Propellers of high-speed ships experience severe damages by wear, which are mainly caused by corrosion and erosion within aggressive saltwater and dissolved sediments. In particular, cavitation erosion plays an important role regarding erosion (Ref 1). The phenomenon is described as the material loss due to the formation and collapse of vapor bubbles by pressure oscillations on the corresponding surfaces (Ref 2). In present, hydrodynamic calculations are carried out in the design phase of ship construction to improve propeller–rudder interactions and thus minimize cavitation. Nevertheless, erosive damage to marine propulsion components cannot be avoided completely (Ref 3). Hence, expensive repairs of the strongly damaged areas are mandatory. These are usually realized by build-up welding and subsequent grinding work (Ref 1, 4).

Arc spraying on the other hand is a simple, very cost-effective spraying technology and determined by a few key

factors (Ref 5, 6). Since the technology is already established for corrosion protection of large structures and on-site repairs (Ref 7, 8), it is also considered for restoration of eroded ship rudders and propellers (Ref 5, 9). Arc voltage and current as well as gas flow, pressure and type primarily affect the final coating quality (Ref 6, 10). In addition, residual stresses in the coatings are strongly influenced by these main parameters and the spray kinematics (Ref 9, 10).

Generally, residual stresses in thermally sprayed coatings arise from the complex superposition of quenching, cooling and other stresses, generated in the spraying process and afterward (Ref 11-13). Quenching stresses mostly occur in spraying technologies with high amounts of thermal energy, which is the case for arc spraying. Initiated by particle impingement during the coating process, this stress component usually appears in tensile form. The particles cannot contract freely in the short cool down phase from the melting temperature due to the rigid substrate surface (Ref 12-14). On the other hand, cooling stresses originate from the thermal mismatch between coating and substrate after the spraying process, which is characterized by different coefficients of thermal expansion (Ref 11, 13, 14). In this way, the cooling stresses cannot be estimated in terms of their magnitude, but at least roughly in terms of their tensile or compressive nature (Ref 15). Varying quenching stresses are reported to dominate the formation of residual stresses in arc-sprayed coatings, although this might be modified by phase changes, e.g., due to heat treatment (Ref 13, 16). Residual stresses in the substrate induced by arc spraying are usually lower than by plasma spraying, but partly show higher gradients in the coatings (Ref 13). This is often attributed to a lower Young's modulus due to a higher porosity compared to other spraying processes and a slightly higher coating thickness (Ref 13).

However, when residual stresses are superimposed by external stresses or coatings exceed a certain thickness, further studies revealed enhanced coating delamination and thus significantly reduced service lives (Ref 13), which was validated by past own investigations (Ref 9). In this study, the residual stress state within the coatings was measured by incremental hole drilling method based on electronic speckle pattern interferometry (ESPI). The non-contact measurement method avoids the time-consuming task of application, wiring and calibration of strain gages on a specimen. Instead, the surface displacements are optically detected utilizing characteristic speckle patterns. These evolve by superposition of object beam and reference beam. By comparison of different sets of phase-shifted images before and after the surface deformations caused by the drilling process, it is possible to determine their sign and size for each pixel. The subsequent analysis with an algorithm includes all pixels in a freely definable ring-shaped area around the drilling hole, which is determined by an inner and outer integration radius. This results in the visualization of the experimentally determined displacements on the surface. Together with the elastic material parameters, especially Young's moduli and Poisson ratio, the stress values can be calculated by the software (Ref 17, 18). Due to the over-determined nature regarding the mathematical background, which is inherent to the measuring method, an additional regularization according to Tikhonov can be carried out or certain pixels exceeding definable threshold values can be excluded from the calculation. More detailed information of the measurement technology is available in literature (Ref 17, 18).

Further findings of the mentioned past investigations (Ref 9), revealed that the classic use of compressed air (Ref 6) resulted on the one hand in large oxides inside the coatings (Ref 9). This negatively affected cavitation erosion resistance of the sprayed aluminum bronze coatings. Furthermore, tensile residual stresses close to the coating surfaces contributed to this material loss (Ref 9). Contrastingly, the use of inert gases or mixtures leads to improved coating qualities (Ref 6, 19, 20). Coatings sprayed using the same materials, parameters and kinematics like in Ref 9 but with a mixture of nitrogen and hydrogen, confirmed these assumptions. The full outcomes are fully described in another own paper (Ref 21). Some of the results recognized were increased cavitation erosion resistance and consequently coating cohesion as well as less residual stresses. Additionally, the change of atomizing gas diminished the impact of the quenching stresses on the coating properties. Additionally, examination of the variation in heat input by the change in spray pattern in Ref 22, using the same setup again, revealed reduced thermal loads during the coating build-up. This resulted in a lower and more even heating of the specimens and reduced tensile stresses for both atomizing gases and bronze materials. Moreover, not only the quantity, but also the course of the residual stresses was changed. Hence, the dominance of the quenching stresses regarding residual stresses and coating properties (Ref 9) was found to be reduced. The use of an alternative gas mixture as atomizing gas diminished the impact of the stresses on the coating properties even further which resembled the findings in Ref 21.

However, all of these experiments were carried out on steel substrates, which at the same time means different coefficients of thermal expansion. According to the mentioned literature, certain amounts of the residual stresses are hence still to be attributed to cooling stresses and actively participate in influencing the coating properties as stated before. The usage of bronze substrates in the present study, in order to cover the topic of propeller repairs at the

same time, could possibly further diminish the influence of the residual stresses this time by reducing the amount of the cooling stresses. This should in turn have an influence on the other coating properties. Just as in Ref 21, a mixture of nitrogen and hydrogen was used as pressurizing gas for the current experiments, while the same parameters and kinematics were used. The results of this study will be compared to the former results on steel substrates, which can be found in detail in Ref 21.

Experimental Methods

Substrate and Coating Materials

The wires for the spray experiments were the cavitation erosion resistant Ni-Al bronze CuAl9Ni5Fe4Mn (Lincoln Electric LNM CuAl8Ni6, Ø 1.6 mm, Ratingen, Germany) and Mn-Al bronze CuMn13Al8Fe3Ni2 (Bedra Bercoweld A300, Ø 1.6 mm, Heuchelheim, Germany). While Mn-Al bronze wires showed a banded structure from wire drawing, the Ni-Al bronze wires were characterized by small precipitates, see also Ref 9.

Substrates of the Ni-Al bronze type were provided and processed by an industrial partner. Due to the limited amount, only one substrate could be coated for each experiment described further down. According to the supplier, the material corresponded to the aluminum bronze CuAl10Fe5Ni5. Hence the mechanical properties should be matching typical values of this alloy, which are very similar to those wire alloys. Some physical and mechanical properties regarding the used materials of this and the past study (Ref 21) can be found in Table 1. The dimensions of the substrates differed somewhat and were about 34 to 36 mm in width, about 70 to 74 mm in height as well as about 48 mm for a single substrate. The thicknesses of Ni-Al bronze substrates were between 4 and 7 mm. Prior to the arc spray process, the substrates were grit-blasted by using corundum of type F24 with a grit size of 600-850 µm.

Arc Spray Experiments

The arc spraying experiments were carried by using a Sulzer Metco Smart Arc prepared with a PPG gun and an HV air cap (Oerlikon Metco Europe GmbH, Kelsterbach, Germany). The spray parameters, a voltage of 28 V, a current of 180 A, a primary atomizing gas pressure of 4 bar and a stand-off distance of 100 mm remained constant throughout all of the experiments. A mixture of nitrogen and 2% of hydrogen was used as atomizing gas. As in the previous studies, three traverse speeds (333 mm/s, 500 mm/s and 666 mm/s) in specimen width direction were used. Moreover, the number of layers was kept identical to the previous experiments, see Table 2. The specimens were clamped inside the mount in front of the spraying gun and fixed with screws from behind. In this way, only a small area was not coated. A meander-shaped type of spray pattern was operated in the experiments.

Deposition Efficiency and Hardness

The deposition efficiency (DE) of the coatings was determined in accordance with ISO 17836.

Additionally, hardness measurements were carried out on the polished surfaces of the coatings by using a Wolpert 432 SVD hardness-testing machine (Wilson Wolpert Instruments, Aachen, Germany, applied load of 9.8 N). A

Table 1 Typical physical and mechanical properties of bronze materials and shipbuilding steel according to Ref 24 and 25

Material specification	Ni-Al bronze CuAl9Ni5Fe4Mn	Mn-Al bronze CuMn13Al8Fe3Ni2	Shipbuilding steel S235JR
Melting range, °C	1050-1080	950-990	> 1536
Tensile strength, MPa	620-740	650-730	> 360
Elongation at break, %	10-22	> 18	> 21%
Young's modulus, GPa	116-124	117	212
Poisson ratio	0.30	0.34	0.30
Coefficient of thermal expansion in 10^{-6} K (0 to 100 °C)	16.3	17.7	11.1
Thermal conductivity, J/s m K	38-42	12.1	54
Electrical conductivity, MS/m	4.4	1.7	6.7

While the substrate properties for this study are very similar to Ni-Al bronze (only slight variation), shipbuilding steel was used for the previous investigations (Ref 21). The properties of the wires, however, correspond to Ni-Al bronze and Mn-Al bronze for both studies

Table 2 Kinematics and primary characteristics of the coatings from the current experiments

	Materials					
	Ni-Al bronze			Mn-Al bronze		
Kinematics						
Traverse speed, mm/s	333	500	666	333	500	666
Number of layers	9 (~)	10 (~)	20 (~)	8 (~)	10 (~)	15 (~)
Primary coating characteristics						
Coating thickness, µm	513(↓)	365 (↓)	580 (~)	491 (↓)	433 (~)	470 (↓)
Standard deviation, µm	14	8	23	35	21	13
Deposition efficiency (DE), %	91.0 (↑)	86.6 (~)	96.6 (↑)	98.2 (↑)	91.9 (↑)	83.4 (~)

Symbols indicate an increase (↑), a decrease (↓) or a stagnation (~) compared to the coatings sprayed on steel substrates (Ref 21)

total of 15 measurements was performed for each specimen in accordance with ISO 6507-1. Subsequently, the ratio of diagonals of the hardness imprints was controlled in order to achieve proper imprints. Thus, solely the seven imprints with the diagonals having the least deviation from each other were chosen. Finally, the minimum and maximum values of these seven measurements were deleted and hence not included in the calculation of mean value and standard deviation—resulting in a series of five sufficient measurements. The described procedure is in accordance with the literature (Ref 23).

Microstructure

Coating quality was investigated by microstructural analyses using an optical microscope (OM) Leica DM6000M (Leica Microsystems GmbH, Wetzlar, Germany), the software tool ImageAccess (Imagic Bildverarbeitung AG, Glattbrugg, Switzerland) and a scanning electron microscope (SEM) JEOL JSM-IT100 (JEOL Germany GmbH, Freising, Germany; acceleration voltage 10 kV, backscatter detector). The specimens for metallographic examinations were hot-mounted via ATM Opal 410 Hot Mounting Press (ATM GmbH, Mammelzen, Germany) and gradually ground and polished (6 µm, 3 µm suspensions, finally oxide polish). The exact coating thicknesses of the specimens, which can be found in Table 2, were determined in the cross sections using five measurements each.

For representative phase analyses, Klemm III color etchant (stock solution: sodium-thiosulphate in water; etching solution: potassium pyrosulphite) was used to improve contrasts in the OM images. Furthermore, energy dispersive x-ray spectrometry (EDS) was executed within the cross sections by using a JEOL Dry SD25 detector (JEOL Germany GmbH, Freising, Germany; acceleration voltage 15 kV). By this, the local chemical composition of the coatings was identified. In particular, the content of oxygen as measure of coating quality was examined by EDS inside the cross sections using the parameters described above. Although not as exact as other testing methods, the chosen setting of the acceleration voltage is a good compromise to detect both light and heavy elements at the same time. Furthermore, the penetration depth and the interaction volume of the electron beam inside the specimens is kept low, which guarantees a near-surface investigation of the freshly polished coatings. Thus, the coatings could be compared to each other in quantitative terms. The coatings examined in Ref 21 were re-evaluated using the same method. Three images (magnification of 500 ×) were investigated for each specimen of the current and the past study.

Electrical Conductivity

The specific electrical conductivity of the specimens was determined by four-terminal method using a Loresta GX MCP-T700 system (Mitsubishi Chemical Analytech Co. LTD, Kanagawa, Japan; PSP measuring head for small specimens; constant current 1 A) with 3 measuring points recording 5 values each. In order to receive a bigger database, the coatings examined in Ref 21 were re-evaluated using the same method, but with 7 values per measuring point. The test method allows to measure the electrical conductivity in the as-sprayed state like for the previous results, while the specimens of the current study were polished before testing.

Cavitation Erosion Behavior

Cavitation erosion behavior was tested for about 120 min in agreement with Ref 2 by using an UIP1000 (Hielscher Ultrasonics GmbH, Teltow, Germany) having a frequency of 19.51 kHz, a peak-to-peak amplitude of 50 µm and a distance from the sonotrode tip to the specimen of 0.5 mm (indirect method). Since surface abnormalities might support crack initiation, the specimens were incrementally

ground and polished (final polish 3 µm) to ensure regular surfaces. Further corresponding to Ref 2, the cumulative mass loss of the specimens (one specimen each) was converted into the cumulative thickness loss, which is also mentioned as mean depth of erosion (MDE). In addition to the material removal itself, various characteristics, such as increases in different areas of the erosion depth-time progress, are usually specified for comparison purposes. In addition to the maximum erosion rate ("MER"), the terminal erosion rate ("TER") is of great importance regarding the long-term stability of a tested material. During the investigations, it was found that thermally sprayed coatings exhibit pronounced peak values at the beginning of the exposure period. These peaks are often far higher than the rapidly emerging terminal erosion rate. Therefore, using the TER as a measure of cavitation resistance of the coatings is more suitable, since it represents the material behavior more exactly. The terminal erosion rate TER was determined by an in-house MATLAB routine in the second half of the test duration of 120 min. The coatings examined in Ref 21 were re-evaluated for the TER values using the same method.

Young's Moduli

The Young's moduli required for the residual stress calculation were determined using a nano-indentation tester NHT (CSM Instruments, Freiburg, Germany, maximum load 50 mN). Due to the inhomogeneous coating structure, a different number of imprints was required for each coating in order to provide a representative analysis. A three-stage, statistical procedure was applied to obtain an identical number of values for each coating, which later on form the mean value and can thus be used for stress analyses. For this purpose, only those values were successively used for the respective calculation of the mean value that showed the smallest relative deviation at that point in the procedure. Other values were deleted and the process was repeated afterward. As a result, five consistent measured values could be used for each final modulus of elasticity. The coatings examined in Ref 21 were re-evaluated using the same method.

Residual Stress Analyses

Residual stress analyses of the coatings were executed by using a Stresstech PRISM system utilizing electronic speckle pattern interferometry (ESPI) and the PrismS software (both Stresstech GmbH, Rennerod, Germany) with three measurements for each specimen. The coatings were tested in the as-sprayed state after the application of a developer spray (typically used in the non-destructive penetration test) to reduce surface reflections. The holes were processed in steps of 50 µm using high-speed steel end mills (2 fluted, TiN coated, Ø 0.8 mm and 1.6 mm) up to a final profile depth of 450 µm. The inner integration radius was 2.5 times the hole diameter, while the outer integration radius corresponded to 4.5 times the hole diameter. The Poisson ratios used for calculation were 0.3 for bulk Ni-Al bronze and 0.34 for bulk Mn-Al bronze (according to Ref 24). A Tikhonov regularization factor of 0.01 was applied in stress calculation. In addition, the integral below the tensile area of the average stress curves was calculated numerically by trapezoidal integration using an in-house MATLAB routine. Due to its nature, this integral shall further on be referred to as the cumulative tensile stress. The stress curves and cumulative tensile stress of the coatings examined in Ref 21 were re-calculated using the re-evaluated values of the Young's moduli.

Results

The following analyses of the present study are compared to former results on steel substrates, which can be found in detail in Ref 21. Since the work presented in Ref 21 was carried out by the same authors, the results are numerically comparable with a high degree of confidence.

Spray Process and Hardness

Regarding the deposition efficiency (DE) slight differences can be observed depending on the material, see Table 2. While the values of Ni-Al bronze show increased DE values for the lowest and highest traverse speed, Mn-Al bronze coatings instead reveal increases for both slower traverse speeds. However, a standard deviation could not be determined due to the reduced number of specimens.

The coating thicknesses are within a range of 365 to 580 µm, which is a wider regime than for the coatings from previous investigations (398 to 594 µm). Ni-Al bronze

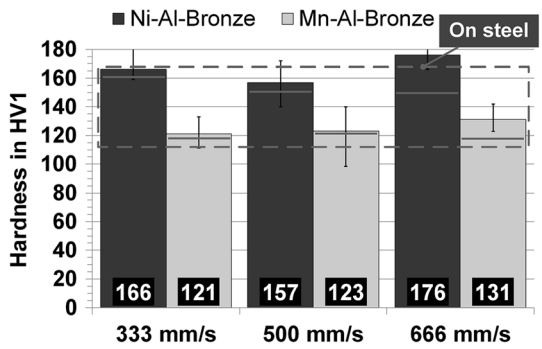

Fig. 1 Average hardness of the coatings from the current experiments. The gray lines indicate the values of coatings sprayed on steel substrates (Ref 21)

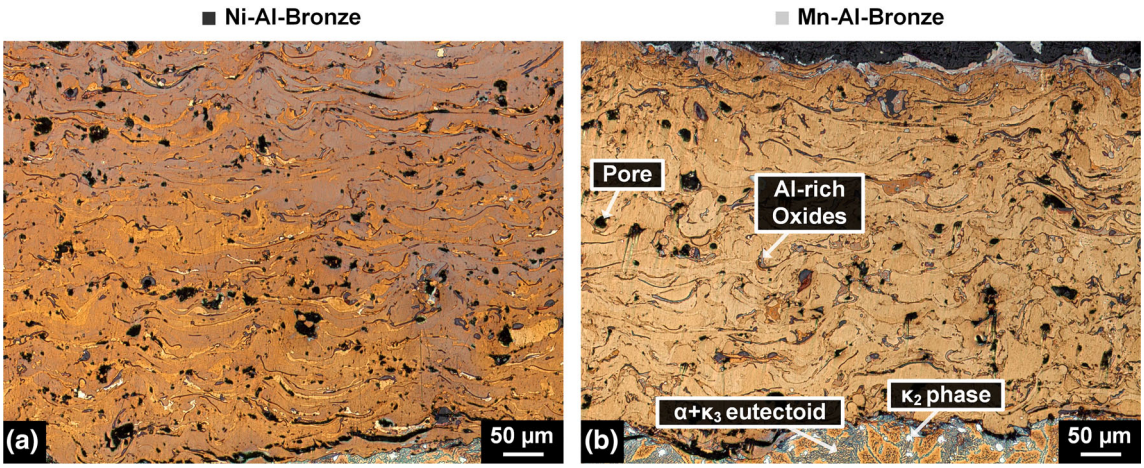

Fig. 2 Representative microstructures of the (a) Ni-Al bronze coatings and (b) Mn-Al bronze coatings as well as the substrate. Small differences in local chemical composition and phase structure are represented by different colors. Both materials mainly consist of lightly etched areas (corresponding to fcc α-phase and intermediate phases) and a certain amount of oxides and pores. Only Mn-Al bronze shows some darkly etched areas (representing ordered β-phase, bcc)

reveals a reduction for both slower traverse speeds, while the thickness is roughly the same for the highest traverse speed. Meanwhile, Mn-Al bronze coatings show almost the same values for 500 mm/s and otherwise a reduction. However, except for one specimen, the standard deviations are higher than for the previously investigated coatings on steel.

Comparing both materials, the hardness values of Mn-Al bronze lie far below the corresponding values of Ni-Al bronze, which is consistent with the trends of the previous investigations, see Fig. 1. Apart from that, both materials exhibit the highest values for the specimens with the highest traverse speed. For the samples of the two slower velocities, on the other hand, no significant differences can be identified, when taking into account the standard deviations. These observations differ from the previous investigations. Furthermore, the values of the two lower traverse speeds are almost identical compared to their counterpart sprayed onto steel, see Fig. 1. Interestingly this differs for the highest traverse speed specimens exhibiting higher values than the comparable coatings on steel.

Representative Microstructural Features

The OM image in Fig. 2 displays the typical microstructures of the color-etched coatings of the Ni-Al bronze (a) and the Mn bronze (b).

The focus on the alloying elements reveals only some local variations in composition, which are highlighted in Fig. 2. In general, the microstructures of the coatings are very similar for both materials exhibiting a certain number of pores as well as oxides. These oxides are primarily formed by Al and appear dark gray, whereas the pores show up in black colors. Solely Mn-Al bronze coatings

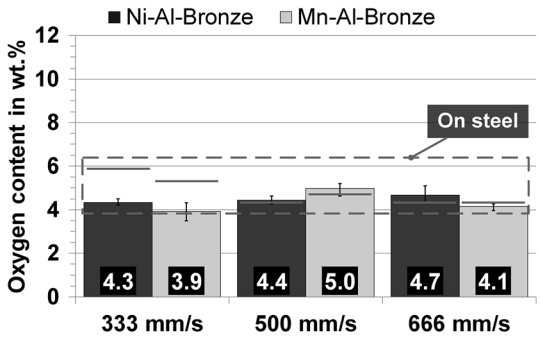

Fig. 3 Oxygen content of the coatings from the current experiments. The gray lines indicate the values of coatings sprayed on steel substrates (Ref 21)

have some darker etched phases, which might could be referred to β-phase or $\alpha + \kappa_3$ eutectoid, see Fig. 2(b). This is in agreement with the previous investigations. However, compared to the substrate structure, which is also visible in Fig. 2, no major precipitates are visible. Indeed, the substrate material shows a pronounced structure with large Fe-rich κ_2 precipitates and wide areas of fine lamellar $\alpha + \kappa_3$ eutectoid. Further on, the substrate microstructure at the interface does not seem to be influenced by the grit blasting process, since no deformations of the grains are to be observed. In comparison with the previous investigations on steel substrates, the coatings appear to have fewer large oxide lamellae at first sight.

Quantitative Microstructural Analyses and Electrical Conductivity

The results of the quantitative oxygen analyses can be found in Fig. 3. The observable trends differ for both materials.

Ni-Al bronze is characterized by nearly unchanged values for the different traverse speeds, when considering the standard deviations. The Mn-Al bronze coatings reveal a higher value at a traverse speed of 500 mm/s, while both other values are almost identical. For those same values, the oxygen contents of Mn-Al bronze coatings are also lower than for the corresponding Ni-Al bronze coatings.

The comparison with the former results on steel substrates in Fig. 3 demonstrates similar values for the coatings with traverse speeds of 500 and 666 mm/s, while both materials show a significant reduction in oxygen content for the lowest traverse speed.

The results of specific electrical conductivity measurements vary strongly for both materials, whereat the 500 mm/s traverse specimens reveal the highest values, which can be seen in Fig. 4. Furthermore, for Ni-Al bronze, the values are in a wider regime than for Mn-Al bronze. Both observations are in agreement with the past study. Different from the previous results, though, the standard deviations are higher for Mn-Al bronze than for Ni-Al bronze. Moreover, all of the coatings show far higher values than the comparable coatings sprayed on steel. Nevertheless, the standard deviations increased too.

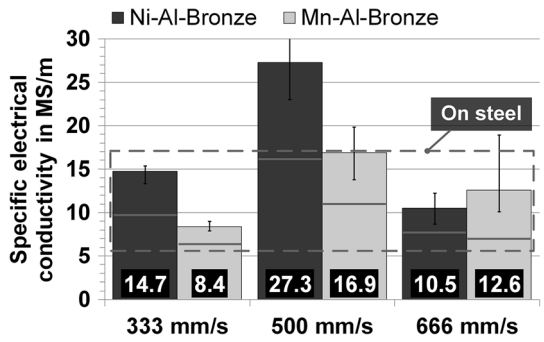

Fig. 4 Specific electrical conductivity of the coatings from the current experiments. The gray lines indicate the values of coatings sprayed on steel substrates (Ref 21)

Cavitation Erosion Behavior

Both materials show similar trends, albeit at slightly different levels of erosion depth, which can be seen in Fig. 5.

The Ni-Al bronze coatings are characterized by a nearly linear progress over the test period, resulting in MDE values in a range between approximately 4 and 8 µm. On the other hand, Mn-Al bronze coatings experience a linear growth to a time of about 60 min. Afterward the curves follow a more asymptotic progress with final MDE between 9 and 11 µm, see Fig. 5. Thus, Ni-Al bronze shows less material loss, which is in agreement with the previous investigations. Furthermore, both materials reveal the trend of increasing MDE with rising traverse speed, while the final erosion depths for the lowest traverse speeds are significantly lower than for the higher ones. This clear trend differs from the previous results. Further compared to the specimens sprayed onto steel substrates, the coatings of the present study have erosion depths reduced in range of approximately 24% up to 74%.

The described trends are confirmed by the calculated erosion rates, which are shown in Fig. 6. The erosion rate TER also increases with increasing traverse speed, while Ni-Al bronze has lower values than Mn-Al bronze. In addition, Mn-Al bronze coatings have higher standard deviations. Again, the lowest traverse speed specimens show much lower values than the specimens of the higher traverse speeds do. Besides, compared to the previous results, the TER is reduced in a range between about 20% up to 72%.

Finally, considering both erosion depth and rate, the Ni-Al bronze coatings exhibit less and more regular material losses as well as erosion rates. As a result, Ni-Al bronze coatings are considered more cavitation erosion resistant.

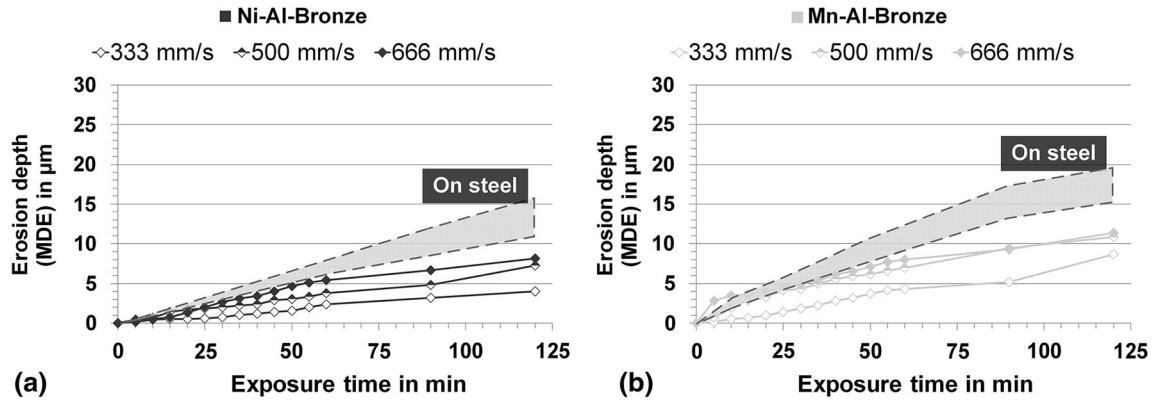

Fig. 5 Erosion depth (MDE) of the coatings from the current experiments. The gray area indicates the values of coatings sprayed on steel substrates (Ref 21)

Moreover, the investigated coatings are more durable than their counterparts on steel substrates are.

Young's Moduli and Residual Stress Analyses

The Young's moduli are crucial for determination of the residual stress state using hole drilling method. At first, the measurements of the Young's moduli differ significantly from bulk material. For cast Ni-Al bronze, the values lie inside a range of 115-121 GPa (Ref 24), while the coatings show far lower average values, which can be seen in Fig. 7.

The Mn-Al bronze coatings reveal an even sharper loss in elasticity than Ni-Al bronze coatings, see Fig. 7. Similar cast Mn-Al bronze alloys have values of about 117 GPa (Ref 24). Both findings are in agreement with the previous study. Additionally both materials reveal a trend of slightly falling moduli with increasing traverse speed, which is more prominent for Mn-Al bronze. In comparison with coatings sprayed on steel, the coating materials show a general decrease in moduli, whereat Ni-Al bronze is affected to a higher extent.

In general, the residual stress curves show a linear decreasing progress of residual tensile stresses up to approximately 300 µm, which is comparable to the coatings sprayed onto steel, see Fig. 8. The highest values can be observed near the surface, reaching up to a maximum of about 240 MPa for both materials. Furthermore, both coating materials show a change in sign for specimens of 500 mm/s traverse speed at a depth roughly corresponding to the coating thickness. In case of Mn-Al bronze, also the coating sprayed with the highest traverse speed has a change to compressive stresses, which does not seem to correlate with coating thickness. Besides, the specimen with the lowest traverse speed shows an almost constant and evenly distributed amount of residual stress over the entire depth profile for both materials. Considering the standard deviations, the stress values near the surface are lower for Mn-Al bronze compared to Ni-Al bronze. Additionally, the curves of Mn-Al bronze cover a wider range of stresses up to a depth of 300 µm, while the curves of Ni-Al bronze can be observed in a narrower regime up to the same depth. This finding is in contrast to the previous results. However, regarding the overall trends of the curves and the sequence of the stress values at the end of the depth

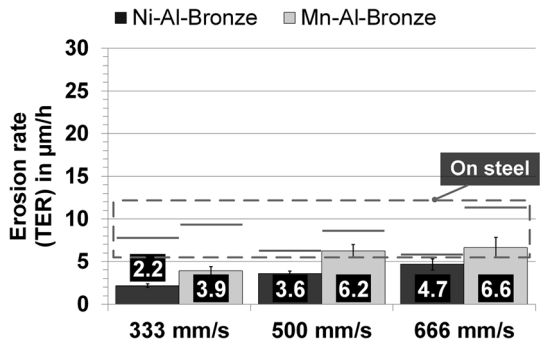

Fig. 6 Terminal erosion rate (TER) of the coatings from the current experiments. The gray lines indicate the values of coatings sprayed on steel substrates (Ref 21)

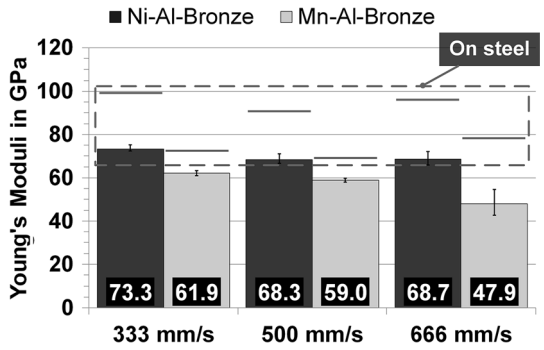

Fig. 7 Average Young's moduli of the coatings from the current experiments. The gray lines indicate the values of coatings sprayed on steel substrates (Ref 21)

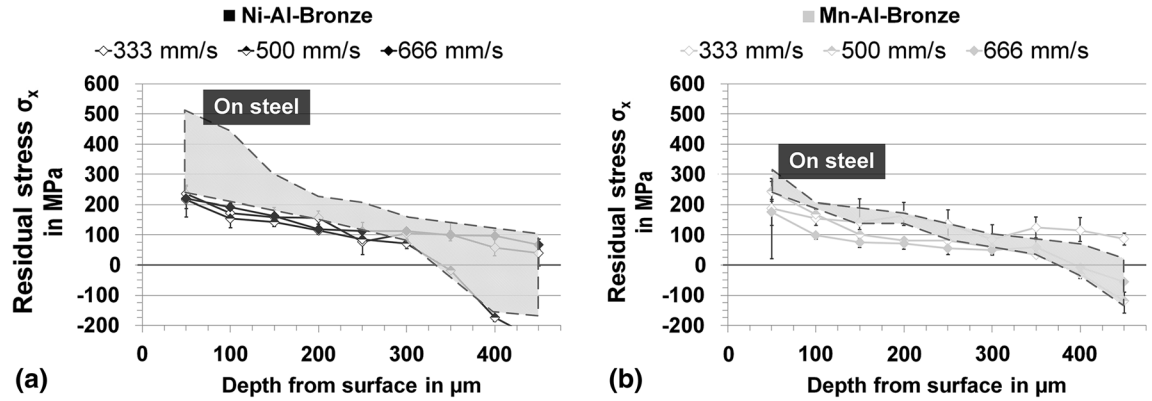

Fig. 8 Residual stresses in specimen width σ_x of the coatings from the current experiments. The gray area indicates the values of coatings sprayed on steel substrates (Ref 21)

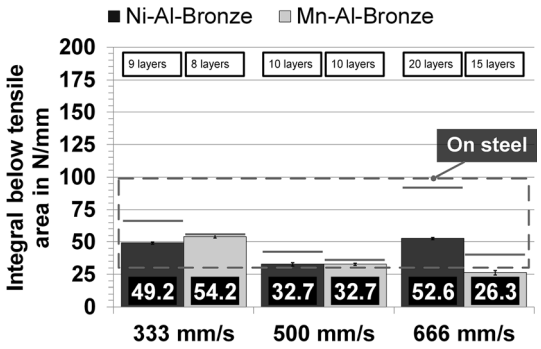

Fig. 9 Average integral below tensile area of the stress curves from the current experiments; calculated by trapezoidal numerical integration. Due to its nature, the integral can also be referred to as the cumulative tensile stress. The gray lines indicate the values of coatings sprayed on steel substrates (Ref 21)

profile, the stresses resemble the previous results. At the same time, compared to the coatings sprayed on steel, the stresses are lowered significantly near the surface up to 300 µm, which is obvious in Fig. 8. Thus, the gradient of the curves seems to be decreased.

The latter is also confirmed by the cumulative tensile stress, which is overall lower compared to the previous investigations, which can be seen in Fig. 9. It must be noted, that Ni-Al bronze is significantly more affected by this reduction than Mn-Al bronze. For both materials, a decrease can be observed from 333 mm/s to 500 mm/s specimens. This reduction of the tensile areas has to correspond to the increasing traverse speeds, since the number of layers is only slightly changed, see Fig. 9. Additionally, a significant increase regarding the number of layers also correlates with a rise in the cumulative tensile stress in case of Ni-Al bronze, which is evident for the change from 500 mm/s to 666 mm/s. The value of 666 mm/s resembles the one for 333 mm/s. In turn, Mn-Al bronze does not reveal such an increase.

Discussion

Interactions with Spray Process and Basic Coating Properties

First, slight changes in deposition efficiency (DE) and coating thickness are evident compared to the previously sprayed coatings on steel in Ref 21 see Table 2. While the DE partly rises, coatings thicknesses tend to be a bit lower. These differences to the coatings sprayed onto steel might be explained by the differences in ductility on the one and heat dissipation on the other hand. While the steel substrates were deformed to a high extent during grit blasting process, the Ni-Al bronze substrates did not seem to be strongly influenced, compare Fig. 2. Furthermore, similar substrate and coating material show comparable properties in terms of thermal expansion. Both probably changes the nature and the formation of the splats by affecting the impact properties of the particles and thus the coating formation due to enhanced flattening and a more homogeneous cooling of the particles. Another point supporting this hypothesis is the presence of smaller and thinner oxides, which might be a secondary consequence of the changed coating formation mechanism. With the highest number of layers, the hardness reaches a maximum too, compare Table 2 and Fig. 1, which is also different from the previous investigations on steel substrates. Possibly the altered coating formation and thus potentially other factors, perhaps even inherited ductility reserves in the form of impact energy, play a role here too. Assuming this, the higher hardness might result from the sharp increase in the number of layers at higher traverse speeds.

Correlation of Residual Stresses, Cohesive Properties and Microstructure

A significantly improved cavitation erosion behavior can be observed for both bronze materials in comparison with the coatings sprayed onto steel in Ref 21, especially for the coatings with the lowest traverse speeds. That is at least partly a consequence of the strongly reduced oxygen content and thus improved cohesion; see "Quantitative Microstructural Analyses and Electrical Conductivity" and "Cavitation Erosion Behavior and Surface Quality" sections. Moreover, the Ni-Al bronze coatings remain superior in comparison with Mn-Al bronze coatings, which might be attributed to the improved microstructure and the intrinsically better cavitation erosion resistance. Nevertheless, oxygen content of the current experiments is almost the same for lowest and highest traverse speed specimen of both materials, see "Quantitative Microstructural Analyses and Electrical Conductivity" section. Therefore, the results of the microstructural analyses cannot explain the improvements in cavitation resistance fully.

In addition, the residual stresses are changed not only in terms of total amount, but primarily also in course and thus also in composition (proportions of quenching and cooling stresses), see chapter "Young's Moduli and Residual Stress Analyses". The lowest traverse speed specimens, while showing the highest cavitation resistance, also reveal the most constant amount of residual stresses throughout the coating, thus reducing the stress gradient. This effect accounts for both materials and results in less stresses near the coating surface, which is important for the application. While the cumulative tensile stresses below the tensile area

are not the lowest for these specimens, they are still far lower than for the corresponding coatings on steel. Here, Ni-Al bronze coatings reach values close to Mn-Al bronze coatings. The strong increase in number of layers for the highest traverse speed also increases tensile stresses in Ni-Al bronze again, albeit having a higher traverse speed. Both can probably be attributed to the strongly reduced component of cooling stresses due to similar coefficients of expansion. Instead, quenching stresses play a greater role, which is evident in the uniform course of the stress curves and in agreement with literature (Ref 13-15). On the contrary, Mn-Al bronze coatings show even some reduction in cumulative tensile stress for the highest number of layers and a wider stress regime overall. This could be a consequence of some portions of remaining cooling stresses due to the slight differences between the two bronze materials. This means that not only tensile residual stresses have a negative effect, but also the gradient within the coating near the surface. This is further confirmed by other own investigations Ref 22, in which the heat input—although on steel substrates—was modified. In this case, too, a more uniform character of the residual stresses had a positive effect on the cavitation erosion resistance. As a result, coatings sprayed with compressed air already achieved very low erosion depths and rates Ref 22.

The measurements of the specific electrical conductivity, however, differ to a very high extent, which may be caused by surface oxidations. Explanations, which have been given in Ref 9, 21 and 22 for combinations of these coatings with steel substrates, obviously cannot be applied to the material combination to a full extent. Thus, it is not entirely clear, if the measurement method is suitable for this material combination. The Young's moduli decrease for both materials by changing the substrate, while the Ni-Al bronze coatings are far more affected than the Mn-Al bronze coatings. This reduction might directly be attributed to the change in coating formation, described in the section before.

Summary

In line with past investigations, the same parameters and kinematics as well as the same mixture of nitrogen and hydrogen as pressurizing gases were used to spray propeller alloys Ni-Al bronze and Mn-Al bronze onto bronze substrates using arc spraying. In order to identify the impact of the change in substrate—for use as a possible means for propeller repair—the results of this study were compared to former results on steel substrates in Ref 21.

The usage of bronze substrates diminished the influence of the residual stresses, this time reducing the amount of cooling stresses to a certain extent, which was visible in the trend of the stress curves and the reduction in the cumulative tensile stress. This in turn had an influence on the various coating properties, but mostly on cavitation erosion resistance. A more regular and even distribution near the substrate surface seems to be of utmost importance for cohesive coating properties. Hence, erosion depths and rates were drastically reduced. On the other hand, the improved bonding between the particles may also contribute to this fact. Moreover, the oxygen contents inside the coatings for the specimens with the lowest traverse speed decreased, which might be a result of a possible change in coating formation, by the change of the substrate, too. Yet, the same conditions led also to reduced Young's moduli and varying trends in hardness and electrical conductivity.

Acknowledgments Open Access funding provided by Projekt DEAL. The authors would like to thank all co-workers involved in the study, namely listed in alphabetical order: B. Ripsch, C. Pust and M. Schulze. Furthermore, the authors thank F. Gärtner for his support and the helpful discussions. The research Project (No. 18449 BG) of the research community Center of Maritime Technologies (CMT), Bramfelder Straße 164, 22305 Hamburg has been funded by the AiF within the program for sponsorship by Industrial Joint Research (IGF) of the German Federal Ministry of Economic Affairs and Energy based on an enactment of the German parliament. This support is highly acknowledged.

References

1. Naval Sea Systems Command and National Surface Treatment Center, Rudder Coating Failures on Navy Ships, 2003. http://slideplayer.com/slide/2373629/. Accessed 17 Jan 2020
2. ASTM, *Standard Test Method For Cavitation Erosion Using Vibratory Apparatus, G32, Annual Book of ASTM Standards*, Vol 03.02, ASTM, Philadelphia, 2010, p 98-116
3. J. Carlton, D. Radosavljevic, and S. Whitworth, Rudder–Propeller–Hull Interaction: The Results of Some Recent Research, In-Service Problems and Their Solutions, in *Proceedings of the First International Symposium on Marine Propulsors—smp'09*, eds. K. Koushan and S. Steen, June 22-24, 2009 (Trondheim, Norway), MARINTEK, 2009, pp. 262-269
4. J. Carlton, *Propeller Maintenance and Repair, Marine Propellers and Propulsion*, 2nd ed., Butterworth-Heinemann, Oxford, 2007, p 511-519

5. J.-H. Kim and M.-H. Lee, A Study on Cavitation Erosion and Corrosion Behavior of Al-, Zn-, Cu-, and Fe-Based Coatings Prepared by Arc Spraying, *J. Therm. Spray Technol.*, 2010, **19**(6), p 1224-1330
6. F. Lang and W. Krömmer, Economic and Ecological Benefits of Using Gas Mixtures for Arc Spraying, in *Proceedings of the 10th Colloquium High Velocity Oxy-Fuel Flame Spraying*, eds. W. Krömmer, October 29-30 (Erding, Germany), Gemeinschaft Thermisches Spritzen e.V. (Association of Thermal Sprayers), 2015, pp. 79-88
7. GTV Verschleißschutz GmbH, Krebs Korrosionsschutz GmbH Rostock, EEW SPC GmbH, Thermal Sprayed Aluminium: a brand-new robot-based technological innovation coating concept (2017). https://www.youtube.com/watch?v=O5v73kPugm0. Accessed 17 Jan 2020
8. A. Barth, Application Areas of Arc Spraying, *Presentation within the Seminar "Modern Coating Technologies"*, Dortmund, Germany, 5th November 2014 (in German)
9. M. Hauer, K. Henkel, S. Krebs, and W. Krömmer, Study of Traverse Speed Effects on Residual Stress State and Cavitation Erosion Behavior of Arc-Sprayed Aluminum Bronze Coatings, *J. Therm. Spray Technol.*, 2017, **26**(1–2), p 217-228
10. J. Chi, A. Zhang, S. Xie, and C. Jin, Process Optimization and Residual Stress Measurement for Arc Spraying Rapid Tooling, *Acad. J. Xi'an Jiaotong Univ.*, 2014, **48**(12), p 126-130 (in Chinese)
11. J. Pina, A. Dias, and J.L. Lebrun, Study by X-ray Diffraction and Mechanical Analysis of the Residual Stress Generation During Thermal Spraying, *Mater. Sci. Eng. A*, 2003, **347**(1–2), p 21-31
12. S. Kuroda, T. Fukushima, and S. Kitahara, Significance of Quenching Stress in the Cohesion and Adhesion of Thermally Sprayed Coatings, *J. Therm. Spray Technol.*, 1992, **1**(4), p 325-332
13. S. Sampath, X.Y. Jiang, J. Matejicek, L. Prchlik, A. Kulkarni, and A. Vaidya, Role of Thermal Spray Processing Method on the Microstructure, Residual Stress and Properties of Coatings: An Integrated Study for Ni–5wt%Al Bond Coats, *Mater. Sci. Eng. A*, 2004, **364**(1–), p 216-231
14. T.W. Clyne and S.C. Gill, Residual Stresses in Thermal Spray Coatings and their Effect on Interfacial Adhesion: A Review of Recent Work, *J. Therm. Spray Technol.*, 1996, **5**(4), p 401-408
15. L. Pawłowski, *The Science and Engineering of Thermal Spray Coatings*, 2nd ed., Wiley, Chichester, 2008, p 255-264
16. Y.X. Chen, X.B. Liang, Y. Liu, S.C. Wei, and B.S. Xu, Effect of Heat Treatment on Microstructure and Residual Stress of Wire Arc Sprayed High Carbon Steel Coating, *Surf. Eng.*, 2010, **26**(6), p 407-412
17. M. Steinzig and E. Ponslet, Residual Stress Measurement using the Hole Drilling Method and Laser Speckle Lnterferometry: Part I, *Exp. Tech.*, 2003, **27**(3), p 43-46
18. G.S. Schajer and M. Steinzig, Full-Field Calculation of Hole-Drilling Residual Stresses from Electronic Speckle Pattern Interferometry Data, *Exp. Mech.*, 2005, **45**(6), p 526-532
19. G. Jandin, H. Liao, Z.Q. Feng, and C. Coddet, Correlations Between Operating Conditions, Microstructure and Mechanical Properties of Twin Wire Arc Sprayed Steel Coatings, *Mater. Sci. Eng. A*, 2003, **349**(1–2), p 298-305
20. X. Wang, J. Heberlein, E. Pfender, and W. Gerberich, Effect of Nozzle Configuration, Gas Pressure, and Gas Type on Coating Properties in Wire Arc Spray, *J. Therm. Spray Technol.*, 1999, **8**(4), p 565-575
21. M. Hauer, K.M. Henkel, S. Krebs, and W. Krömmer, Alternative Gas Mixtures in Arc Spraying: A Chance to Improve Coating Properties and Residual Stress States, *J. Therm. Spray Technol.*, 2018, **27**(1–2), p 106-118
22. M. Hauer, R. Banaschik, W. Krömmer, and K.M. Henkel, Variation of Heat Input and Its Influence on Residual Stresses and Coating Properties in Arc Spraying with Different Gas Mixtures, *J. Therm. Spray Technol.*, 2019, **28**(1–2), p 40-52
23. H. Mathesius and W. Krömmer, *Praxis des thermischen Spritzens: Anleitung für das Fachpersonal*, 2nd ed., DVS Media GmbH, Düsseldorf, 2014, p 107 ((in German))
24. H.J. Meigh, *Cast and Wrought Aluminium Bronzes: Properties, Processes and Structure*, Copper Development Association/IOM Communications, London, 2000, pp. 3-31, 293-351
25. Thyssenkrupp Materials Services GmbH, Material data sheet S235Jxx, MX/TIS-TS_12.2017 (2017) (in German). https://de.materials4me.com/media/pdf/95/cf/4a/Werkstoffdatenblatt_S235JR_1-0038_01-2020.pdf. Accessed 17 Jan 2020